Peer reviewed version

Link to published version (if available):
10.1109/ICoSC.2018.8587807

Link to publication record in Explore Bristol Research
PDF-document

University of Bristol - Explore Bristol Research
General rights

Reconciling Full-Order LPV Design and Augmented Structured $\mathcal{H}_\infty$ via Internal Model Principle: a Launch Vehicle Application*

Diego Navarro-Tapia[1], Andrés Marcos[1], Samir Bennani[2] and Christophe Roux[3]

Abstract— This article presents an indirect method to characterize a wind disturbance internal model that can be used to augment the capabilities of a classical controller structure for the atmospheric-phase thrust vector control (TVC) system of the VEGA launcher. This characterization is based on a comparison between a structured $\mathcal{H}_\infty$ and a full-order LPV controller with better performance levels. The identified wind model is then explicitly employed to re-design the structured $\mathcal{H}_\infty$ controller in order to achieve similar levels as the full-order LPV controller. This design reconciles the current VEGA control system architecture with the internal model principle, which states that a controller must have structural features to contain the internal model of the signal to be controlled. The effect of this new controller structure is analysed in terms of robust stability and performance using the singular structured value μ technique. The results show that embedding the internal model structure in the control system provides an extra degree of freedom to improve the launcher performance against wind gusts.

I. INTRODUCTION

Wind disturbance rejection is one of the main factors that must be addressed by the ascent-flight control system of any launch vehicle. This is because the control performance of the atmospheric phase is heavily impacted by wind-induced structural loads which may cause instability and loss of control. Indeed, the classical control synthesis strategies are driven by the ability to reduce the wind disturbance action in the main control channels (i.e. attitude-error-minimum, drift-minimum and load-minimum control modes) [1].

For adequate disturbance rejection, the control system must contain the necessary structure to encapsulate a model of the disturbance dynamics. This is also known as the internal model principle (IMP) [2]. The IMP can be managed via the classical internal model control (IMC) [3], which consists of parametrizing the controller to include an explicit model of the process to be controlled (tracking reference, plant, disturbance) and also by including a wind disturbance observer in the closed-loop system [4].

This internal model (IM) structure is created implicitly when using full-order robust control synthesis techniques such as the standard (i.e. non-structured) $\mathcal{H}_\infty$, μ or linear parameter varying (LPV). Nevertheless, these methods result in high-order designs and do not allow to explicitly define a structure for the controller. This is an important limitation in aerospace applications where a good understanding of the controller structure is appreciated.

The previous limitation can be overcome by using the structured $\mathcal{H}_\infty$ technique [5] as it enables specifying the structure of the controller for design. This synthesis approach allows to reconcile classical control architectures with robust control design and analysis techniques [6], [7]. Furthermore, it has been widely used in the last decade, resulting in relevant Space flown missions such as the Rosetta's orbit controller tuning [8], piloted flight tests [9] and launch vehicle control design [10], [11].

Nevertheless, to get an accurate wind disturbance rejection using this structured technique, the designer must embed explicitly the IM structure. The aim of this work is to show how to characterize such an IM model for the atmospheric ascent phase of the VEGA launcher, and also to show how to effectively use it within the VEGA thrust vector control (TVC) design. The process followed leverages the knowledge from a full-order LPV control design and a baseline structured $\mathcal{H}_\infty$ design (obtained using the actual VEGA launcher TVC architecture).

The layout of the paper is as follows: Section II briefly describes the VEGA launch vehicle and presents the uncertainty modelling approach. In Section III, the process and model followed to identify a wind/gust rejection IM is presented. Then, a structured $\mathcal{H}_\infty$ design including the IM architecture is performed in Section IV. Section V analyses the robust stability and performance of this new design using the structured singular value technique. Finally, Section VI ends with the conclusions.

II. VEGA LAUNCH VEHICLE

A. VEGA launch vehicle and mission

VEGA launcher is the new European Small Launch Vehicle developed under the responsibility of the European Space Agency (ESA) and European Launch Vehicle (ELV S.p.A.) as prime contractor. VEGA is a single-body launcher, which follows a four-stage approach. All stages are controlled using a TVC system and a roll and attitude control system (RACS) during the propelled phases.

The launcher has successfully performed twelve launches since its maiden flight on 13th February 2012. In particular, in this work the design and analysis are applied to the actual VEGA VV05 mission data [12].

[1] Diego Navarro-Tapia and Andrés Marcos are with the Technology for Aerospace Control (TASC) Lab., Department of Aerospace Engineering, University of Bristol, BS8 1TR, United Kingdom diego.navarro-tapia/andres.marcos@bristol.ac.uk
[2] Samir Bennani is with ESA-ESTEC, Noordwijk, 2201AZ, The Netherlands samir.bennani@esa.int
[3] Christophe Roux is with AVIO, VEGA GNC Department, Colleferro, 00034, Italy Christophe.Roux@avio.com

B. Launch vehicle model

The VEGA launcher model is represented by the standard 6 degrees-of-freedom equations of motion [6]. This model contains the main rigid-body motion described by the translational and rotational dynamics of the vehicle, the nozzle dynamics also known as tail-wags-dog (TWD) and the flexible-body motion representing the elastic behaviour of the launch vehicle. In addition, other contributions such as the sensors characterization and wind disturbance dynamics are also considered. Note that due to axial symmetry, the same control law is employed for pitch and yaw axes under the assumption that they are decoupled. Thus, for analysis and design purposes, this paper focuses on the yaw axis.

All relevant dynamics are expressed as a state-space representation and then augmented to incorporate parametric uncertainties using the linear fractional transformation (LFT) theory [13]. The VEGA LFT model is built using additive parametric uncertainties defined as $x = x^0 + \sigma_x^\# \delta_\#$, with x^0 the nominal value of parameter x and $\sigma_x^\#$ its level of uncertainty with respect to the norm-bounded uncertainty flag $\delta_\#$. The LFT modelling approach used in this work identifies a reduced set of uncertainty flags that captures the uncertain behaviour of the system (for further details on this modelling strategy, the reader is referred to reference [14]). The resultant uncertainty set is described in equation 1, and is formed by 6 rigid-body scattering flags: combustion time δ_{dTc}, atmospheric density δ_ρ, and dispersions and uncertainties for the normal aerodynamic coefficient (δ_{dispCN}, δ_{uncCN}) and the center of pressure x-coordinate ($\delta_{dispX_{CP}}$ and $\delta_{uncX_{CP}}$); and 5 flexible-body scattering flags: bending frequencies δ_{ω_q} and rotations and translations at the nozzle pivot point (PVP) and the inertial navigation system (INS) ($\delta_{\Psi_{PVP}}, \delta_{\Psi'_{PVP}}, \delta_{\Psi_{INS}}, \delta_{\Psi'_{INS}}$).

$$\mathbf{\Delta_{LV}} = \Big\{ \text{diag}(\delta_{dTC}\mathrm{I}_{56}, \delta_\rho\mathrm{I}_4, \delta_{dispCN}\mathrm{I}_2, \delta_{uncCN}\mathrm{I}_2, \delta_{dispX_{CP}}\mathrm{I}_6,$$
$$\delta_{uncX_{CP}}\mathrm{I}_6, \delta_{\omega_q}\mathrm{I}_6, \delta_{\Psi_{PVP}}\mathrm{I}_4, \delta_{\Psi'_{PVP}}\mathrm{I}_5, \delta_{\Psi_{INS}}\mathrm{I}_2, \delta_{\Psi'_{INS}}\mathrm{I}_2);$$
$$\delta_\# \in \mathbb{R}; ||\delta_\#||_\infty \leq 1 \Big\} \quad (1)$$

To illustrate the LFT model range, the frequency response of the nominal VEGA attitude channel at t=50s is compared with 1000 random scattered responses in Figure 1a.
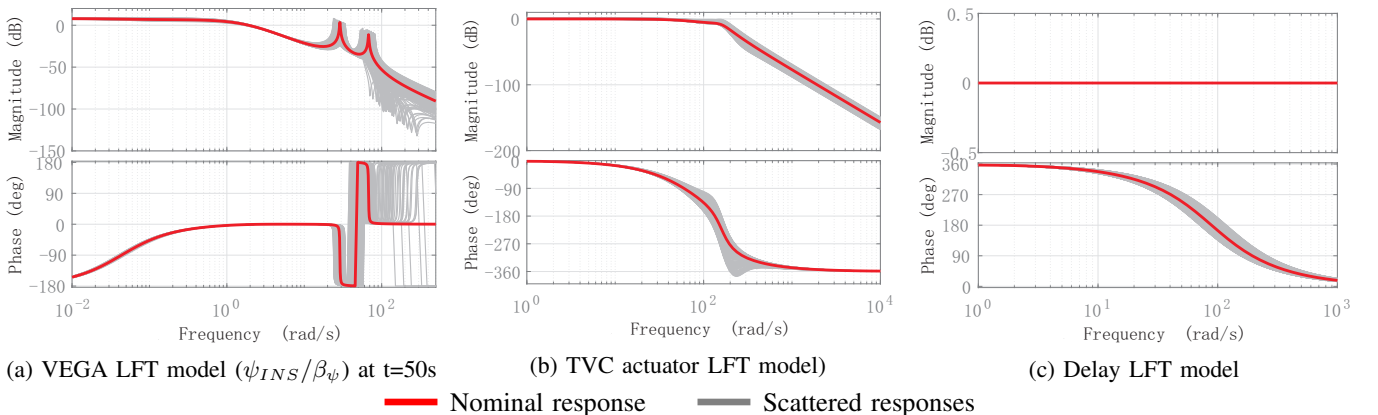
The VEGA LFT model can be represented as an upper LFT interconnection (see Figure 2) also denoted as $\mathcal{F}_u(G_{LV}(s), \Delta_{LV})$, where $G_{LV}(s)$ describes the known part of the model and the uncertainty matrix Δ_{LV} belongs to the set $\mathbf{\Delta_{LV}}$. The model uses three inputs ($\mathbf{u_{LV}} = \begin{bmatrix} \beta_\psi & \ddot{\beta}_\psi & v_w \end{bmatrix}^T$), with β_ψ and $\ddot{\beta}_\psi$ the nozzle deflection angle and its acceleration and v_w the wind disturbance velocity; and five outputs ($\mathbf{y_{LV}} = \begin{bmatrix} Q\alpha & \psi_{INS} & \dot{\psi}_{INS} & z_{INS} & \dot{z}_{INS} \end{bmatrix}^T$), which include the load performance indicator $Q\alpha$ (with Q the dynamic pressure and α the angle of attack), and the drift z, yaw attitude ψ and their derivatives measured at the inertial navigation system (INS) node location.
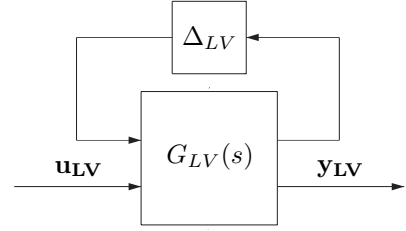

Fig. 2: VEGA LFT model

C. Actuation model

The actuation chain system is composed of two models:

1) TVC actuator model: it characterizes the dynamics of the TVC actuators obtained from hardware-in-the-loop simulations. This model is also represented as a LFT interconnection $\big(\mathcal{F}_u(G_{TVC}(s), \Delta_{TVC})$ with $\Delta_{TVC} \in \mathbf{\Delta_{TVC}}\big)$ to account for actuator uncertainties. A detailed description of the uncertainty set $\mathbf{\Delta_{TVC}}$ and the TVC dynamics can be found in reference [15]. The coverage of this LFT model is shown in Figure 1b.

2) Delay model: it represents the delays introduced by the on-board computers, sensors and hardware (see Figure 1c). This model is also expressed as an upper LFT representation ($\mathcal{F}_u(G_\tau(s), \Delta_\tau)$), where $G_\tau(s)$ is approximated by a second order Padé transfer function and $\Delta_\tau \in \mathbf{\Delta_\tau}$ with $\mathbf{\Delta_\tau} = \big\{ \delta_\tau \mathrm{I}_4; \delta_\tau \in \mathbb{R}; ||\delta_\tau||_\infty \leq 1 \big\}$.

(a) VEGA LFT model (ψ_{INS}/β_ψ) at t=50s
(b) TVC actuator LFT model)
(c) Delay LFT model

——— Nominal response ——— Scattered responses

Fig. 1: Bode plots of the uncertain LFT models

III. STRUCTURED VS FULL-ORDER DESIGN

In this section, a robust structured $\mathcal{H}_\infty$ design and a full-order LPV controller are presented and compared to identify the internal model structure.

A. Robust structured $\mathcal{H}_\infty$ design

This controller was designed using the structured $\mathcal{H}_\infty$ control approach [5] and the actual VEGA TVC architecture [16]. Unlike the state-of-practice where the design of the rigid-body controller and bending filters are traditionally addressed sequentially in several iterative steps, for this design, the rigid-body controller and bending filter were parametrized and tuned simultaneously. This joint design allows to optimize the rigid-body performance while achieving an adequate bending mode attenuation. In addition, it simplifies the synthesis process and reduces the tuning effort prior to each mission. It is important to remark that this design was performed taking parametric uncertainties into account. The reader is referred to reference [7] for further details about the synthesis process of this controller.

The control problem was formulated as the standard $\mathcal{H}_\infty$ design interconnection illustrated in Figure 3. The closed-loop interconnections are re-arranged into the generalised plant $P(s)$, which gathers the LFT models presented in Section II. Note that all the uncertainty blocks are pulled out of this plant as an upper LFT and the uncertainty matrix Δ is defined in the set $\mathbf{\Delta} = diag(\mathbf{\Delta_{LV}}, \mathbf{\Delta}_\tau, \mathbf{\Delta_{TVC}})$. The generalised plant $P(s)$ has a set of exogenous inputs $\mathbf{d}$, which combines commands, wind disturbance and sensor noise inputs; and a set of exogenous outputs defined as $\mathbf{e} = \begin{bmatrix} \psi_e & \psi_{INS} & z_{INS} & \dot{z}_{INS} & Q\alpha & \beta_{\psi c} \end{bmatrix}^T$. And finally, the vector $\mathbf{y} = \begin{bmatrix} \psi_e & \dot{\psi}_e & z_e & \dot{z}_e \end{bmatrix}^T$ represents the inputs of the controller $K(s)$, while the controller output is denoted by the scalar $u = \beta_{\psi c}$.
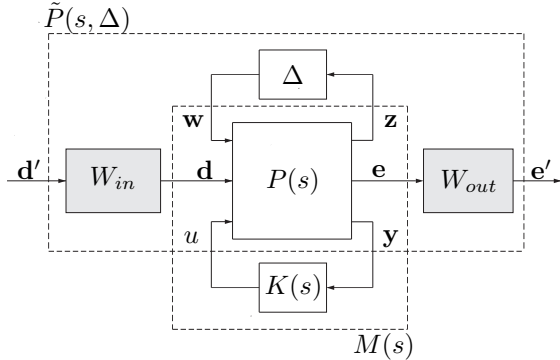

Fig. 3: Robust standard $\mathcal{H}_\infty$ interconnection

The TVC structure of this design is illustrated in Figure 4a, where all components are tunable and represented in shaded blocks. The rigid-body controller is composed of 4 rigid-body gains. In addition, a bending filter $H_3(s)$, which notches the first bending mode and attenuates the upper modes, is also included in the architecture. In total, this design has 15 states and the rigid-body gains and the bending filter $H_3(s)$ parameters are gain-scheduled using the non-gravitational velocity (VNG) as a scheduling parameter, which is the actual VEGA scheduling variable [16].
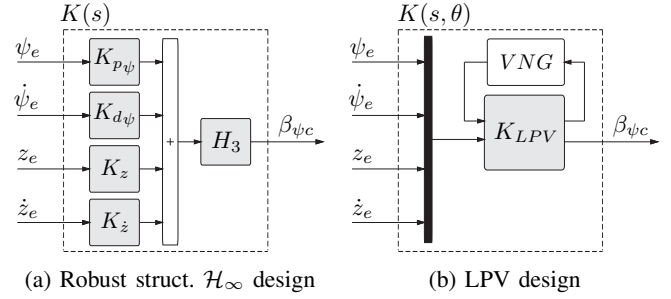

(a) Robust struct. $\mathcal{H}_\infty$ design (b) LPV design

Fig. 4: TVC structure for the VEGA control designs

B. LPV design

This controller was designed using the LPV synthesis technique [17]. This approach allows taking into account the varying behaviour of the system as captured by a measured parameter θ. Different scheduling parameters were tested but for proper comparison to the previous design, the same VNG parameter is used, but also using its known rate bound defined by the non-gravitational acceleration. The detailed synthesis process of this design is provided in reference [18].

This controller results in a full-order 22-states controller K_{LPV} (see Figure 4b), which includes the rigid-body controller and bending filters functionalities.

C. Comparison

As previously mentioned, full-order control synthesis techniques implicitly encapsulate the IM in the resultant controller as they absorb all the dynamics used for the design. The LPV design was developed to showcase the advantages of this type of techniques over the classically ad-hoc gain-scheduled approaches.

When comparing the frequency responses of the previous two designs and the baseline controller used for the actual VEGA VV05 mission (see Figure 5), it becomes clear that the LPV design has a wind disturbance IM that is missing in the other. It is observed that the LPV design performs a derivative action at low frequencies, which is the frequency range where the wind disturbance input has a major effect. This characteristic is noticeable in all the controller channels but the attitude rate error, where the derivative response is minimal.

Thus, due to the easily augmenting capabilities of the structured $\mathcal{H}_\infty$ approach, it was decided to characterize this wind/gust IM model and assess its reusability for the redesign of the structured $\mathcal{H}_\infty$ controller. The latter will be presented later in Section IV. In this work, this IM structure is roughly approximated as a first-order high-pass filter at low frequencies. In addition, it is notable that the LPV design presents higher drift-rate gains than the other controllers. This feature generally leads to a better drift-rate performance against wind disturbance, which in turn improves the wind rejection performance of the $Q\alpha$ channel (recall that the angle of attack α depends directly on the drift-rate). This wind rejection performance will be further analysed in the next section.
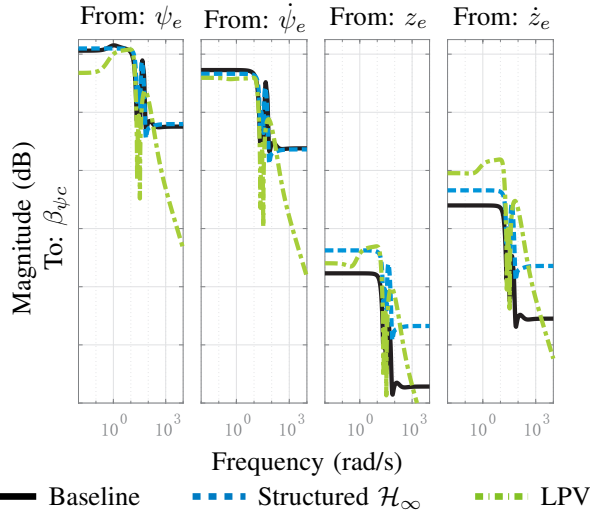
Fig. 5: Bode plot controller comparison at t=50s

Fig. 7: Allowable frequency responses for $H_{IM}(s)$

IV. STRUCTURED $\mathcal{H}_\infty$ DESIGN WITH INTERNAL MODEL

In this section, the previous structured $\mathcal{H}_\infty$ controller is re-designed but incorporating the identified wind internal model. For this article, the focus and presentation is for the LTI controller designed at time t=50s (i.e. maximum dynamic pressure).

A. Problem formulation

The control problem is formulated in the same manner as the standard $\mathcal{H}_\infty$ design interconnection illustrated in Figure 3. In this case, the defined structure of the controller $K(s)$ is illustrated in Figure 6. With respect to the structured $\mathcal{H}_\infty$ controller of Section III-A (see Figure 4a), in here $K(s)$ embeds the internal model denoted as $H_{IM}(s)$. Using this configuration, the derivative action will be applied to all the controller channels, as opposed to the full-order LPV design (see Figure 5). Similarly, tunable components are represented as shaded blocks. Note that for design simplicity the filter $H_3(s)$ is kept as for the robust structured $\mathcal{H}_\infty$ design presented in Section III-A.
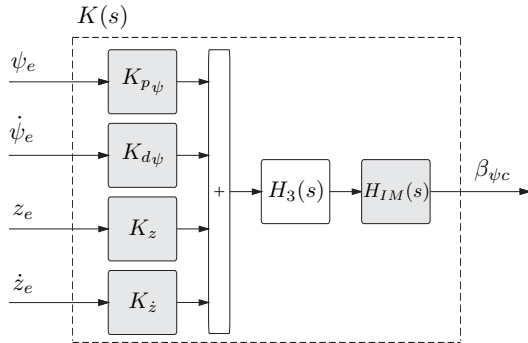

Fig. 6: TVC structure for the IM-based structured $\mathcal{H}_\infty$ design

As mentioned before, the internal model $H_{IM}(s)$ is characterized by a first-order high-pass transfer function. The action of this new controller structure is limited to low frequency by constraining the allowable values (minimum and maximum) of the tunable pole and zero parameters. Figure 7 shows the allowable frequency responses for $H_{IM}(s)$.
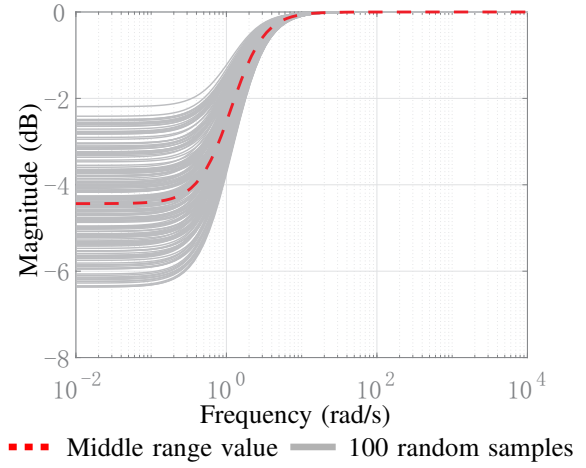
As for the weighting functions, it should be remarked that this design uses the same weight configuration as the one in reference [7]. Only two weighting functions have been changed: 1) since the bending filter is not tuned, the output actuation weight is simplified as a low-pass filter; 2) the output drift-rate requirement is set tighter in order to emulate the $Q\alpha$ wind rejection performance described in the last section. Due to space limitations, the weighting functions used are not shown.

The structured $\mathcal{H}_\infty$ control problem consists of finding a stabilizing structured controller $K(s)$ that minimises the cost function $\min_{K(s)} ||\mathcal{F}_l(\tilde{P}(s, \Delta), K(s))||_\infty$, where $\tilde{P}$ is the augmented generalised plant (see Figure 3).

B. Nominal analysis

Figure 8 compares the Bode plots of the new design with the other controllers. Looking at the IM-based responses (in red), it is worthy noticing the high-pass action at low frequencies added by including in the design the internal model.
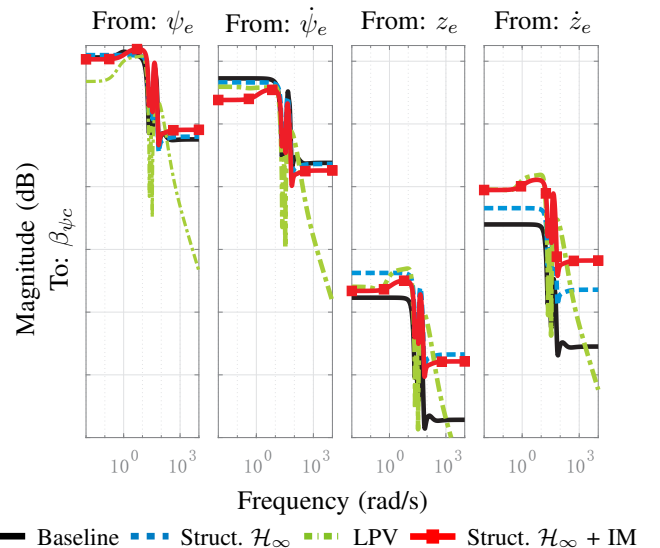

Fig. 8: Bode plot controller comparison at t=50s

Furthermore, it is also observed that the augmented design presents similar drift-rate gains as the LPV controller. As stated in Section III, this behaviour results in an improved $Q\alpha$ wind rejection performance. To support this analysis, the frequency responses of the $Q\alpha$ channel from the wind disturbance input are shown for all the controllers in Figure 8. This plot shows that the structured IM-based and LPV designs (see red and green responses) achieve a significant reduction of the $Q\alpha$ transient energy between 0.1 and 1 rad/s, which is precisely the range of action of the IM. Note that this level of wind rejection cannot be achieved by the baseline or the structured $\mathcal{H}_\infty$ controllers because higher drift-rate gains would imply a deterioration of the rigid-body stability gain margins. Although it is recognized that this improvement is achieved at the expense of worsening the performance for very low- and high-frequency wind gusts, a campaign of simulations using the nonlinear, high-fidelity simulator with different wind profiles indicates that the $Q\alpha$ deterioration at those frequencies is not critical.
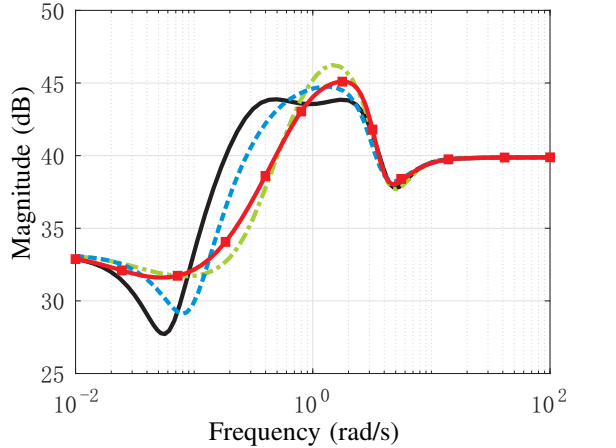

Fig. 9: Bode plots of the $Q\alpha$ channel from wind input at t=50s

V. ROBUST ANALYSIS

This section analyses the robustness characteristics of the internal-model-based structured $\mathcal{H}_\infty$ design with respect to the VV05 baseline and the controllers in Section III.

A. Robust stability analysis

The robust stability of the closed-loop system, defined as the upper LFT interconnection $\mathcal{F}_u\big(M(s), \Delta\big)$ with $M(s) = \mathcal{F}_l\big(P(s), K(s)\big)$, can be assessed via the singular structured value [19]:

$$\mu_\Delta(M_{11}) = \frac{1}{min_\Delta\{\overline{\sigma}(\Delta):det(I-M_{11}\Delta)=0\}} \quad \text{with} \ ||\Delta||_\infty < 1 \tag{2}$$

where M_{11} represents the transfer function from the uncertainty channel **w** to **z** (see Figure 3).

This robust analysis technique provides analytical guarantees that the system $M(s)$ is robustly stable if $\mu_\Delta\big(M_{11}(s)\big) \leq 1$ over all frequencies. This implies that

there is no combination of uncertainties within the set Δ which leads to instability. Note that μ is computed using bounds because the singular structured value computation is a non-polynominal hard problem [19]. The upper bound (UB) provides the maximum size perturbation for which the RS condition shown in equation 2 is violated, while the lower bound (LB) provides the minimum size perturbation for which the RS condition is guaranteed. In order to improve the accuracy of the μ computation, the uncertainty matrix Δ has been modified to include a 1% complex uncertainty to one of the TVC uncertain parameters.

Figure 10 shows the upper bound of μ computed at t=50s for the different controllers. All the designs satisfy the RS condition at all frequencies. Comparing both structured $\mathcal{H}_\infty$ designs, it is observed that the augmented design achieves a reduction of RS at low frequencies at the expense of slightly increasing μ at mid frequencies where the wind contribution is smaller. It is worthy noticing that this improvement at low frequencies comes from the high-pass action performed by the internal model (see Figure 7).
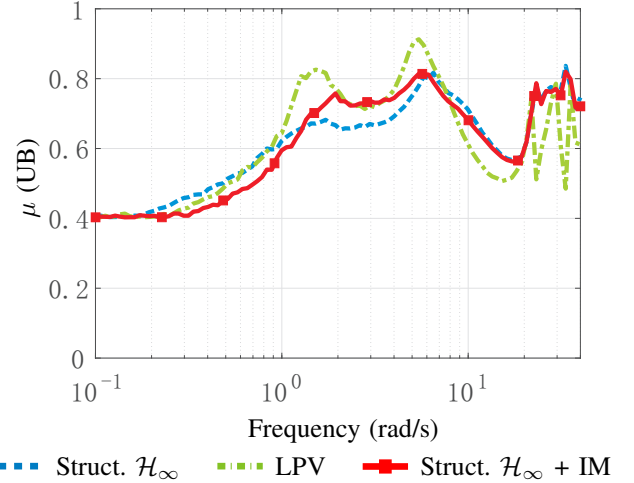

Fig. 10: RS analysis at t=50s

B. Robust performance analysis

The structured singular value can also be used for robust performance (RP) analysis, which verifies if the performance objectives defined by the weighting functions are satisfied for all the plants in the uncertainty set defined by the LFT models. To that end, the robust design interconnection of Figure 3 must be closed using a fictitious full-complex perturbation matrix Δ_P, which does not represent any actual perturbation of the system [19]. In this framework, RP is guaranteed if $\mu_{\hat{\Delta}}\big(N(s)\big) < 1$ over all frequencies, where $N(s) = W_{in}M(s)W_{out}(s)$ and $\hat{\Delta} = diag(\Delta, \Delta_P)$. Furthermore, it is well-known that RP values are directly related to RS and also to the maximum singular value, which represents nominal performance (NP), through equation 3 [20]. Thus, it is expected that the RP results follow the same trend observed for RS.

$$\underbrace{\mu_{\hat{\Delta}}}_{RP} \geq max\Big\{\underbrace{\mu_\Delta(N_{11})}_{RS}, \underbrace{\sigma(N_{22})}_{NP}\Big\} \tag{3}$$

This analysis framework allows to analyse the effect of the different system inputs (tracking command, wind disturbance, noise) on RP. For this case, the analysis is focused on the $Q\alpha$ robust performance from the wind disturbance input. Figure 11 shows the upper bound of μ for the different controllers. The same trend as before is recognized here. The augmented design with the internal model achieves a better RP with respect to the structured $\mathcal{H}_\infty$ controller at low frequencies at the expense of very slight increase of the RP at mid frequencies where the wind has less effect. It should be reminded that these results are based on the specific weights used for the design of the augmented structured $\mathcal{H}_\infty$ design.
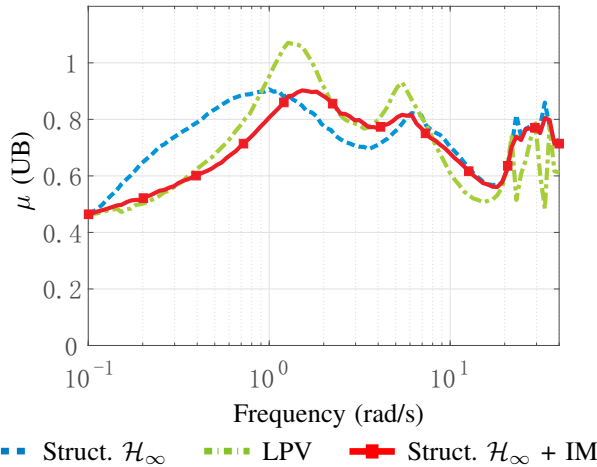

Fig. 11: RP analysis of $Q\alpha$ channel from wind disturbance at t=50s

VI. CONCLUSIONS

In this article, the internal model principle is applied to the design of the atmospheric control system of the VEGA launcher. The main idea of this principle is that the controller must have the necessary structure to perform adequate wind disturbance rejection control.

A wind disturbance internal model is identified by comparing the control architecture of a structured $\mathcal{H}_\infty$ controller with a full-order LPV design, which encapsulates this model implicitly by design. From this comparison, the identified model is characterized as a high-pass filter at low frequencies.

In order to study the effect of the internal model, the structured $\mathcal{H}_\infty$ approach is used again to re-design the controller at a linear operating point but now incorporating in its structure the internal model. For this design, the internal model is parametrized as a first-order transfer function, whose tunable pole and zero parameters are configured to perform a high-pass action at low frequencies.

Finally, robustness characteristics of this new design are analysed using the singular structured value μ. The results show that the introduction of the internal model achieves a better robust stability at low frequencies, which is the frequency range where the wind disturbance has more impact. Indeed, this coincides with the actual internal model bandwidth. Overall, it can be concluded that the internal model enhances the nominal and robust wind rejection performance capabilities of the current VEGA control system architecture. Finally, it is highlighted that the augmented design with 16 states manages to improve overall the robust stability and performance in comparison to the full-order LPV design with 23 states.

REFERENCES

[1] R. Hoelker, *Theory of artificial stabilization of missiles and space vehicles with exposition of four control principles.* NASA Technical Note TN D-555, 1961.
[2] B. Francis and W. Wonham, "The internal model principle of control theory," *Automatica*, vol. 12, no. 5, pp. 457 – 465, 1976.
[3] M. Morari and E. Zafiriou, *Robust Process Control.* Prentice-Hall, 1989.
[4] H. Shim, G. Park, Y. Joo, J. Back, and N. H. Jo, "Yet another tutorial of disturbance observer: robust stabilization and recovery of nominal performance," *Control Theory and Technology*, vol. 14, no. 3, pp. 237–249, Aug 2016.
[5] P. Gahinet and P. Apkarian, "Structured $\mathcal{H}_\infty$ Synthesis in MATLAB," in *Proceedings of the 18th World Congress of the International Federation of Automatic Control (IFAC)*, vol. 18, August 2011, pp. 1435–1440.
[6] D. Navarro-Tapia, A. Marcos, S. Bennani, and C. Roux, "Structured $\mathcal{H}_\infty$ control design for the VEGA launch vehicle: Recovery of the legacy control behaviour," in *Proceedings of the 10th International ESA Conference on Guidance, Navigation and Control Systems (ESA-GNC)*, May 2017.
[7] ——, "Joint robust structured $\mathcal{H}_\infty$ design of VEGA launcher's rigid-body controller and bending filter," in *Proceedings of the 69th International Astronautical Congress (IAC)*, oct 2018.
[8] A. Falcoz, C. Pittet, S. Bennani, A. Guignard, C. Bayart, and B. Frapard, "Systematic design methods of robust and structured controllers for satellites," *CEAS Space Journal*, vol. 7, no. 3, pp. 319–334, 2015.
[9] A. Marcos and M. Sato, "Flight testing of an structured $\mathcal{H}_\infty$ controller: an EU-Japan collaborative experience," in *Proceedings of the 1st IEEE Conference on Control Technology and Applications (CCTA)*, August 2017, pp. 1590–1595.
[10] D. Saussié, Q. Barbès, and C. Bérard, "Self-Scheduled and Structured $\mathcal{H}_\infty$ Synthesis : A Launch Vehicle Application," in *Proceedings of the American Control Conference (ACC)*, June 2013, pp. 1590–1595.
[11] M. Ganet-Schoeller, J. Desmariaux, and C. Combier, "Structured Control for Future European Launchers," *AerospaceLab Journal*, no. 13, pp. pages 1–10, Nov. 2017.
[12] Arianespace, "VEGA flight VV05," June 2015, http://www.arianespace.com/mission/vega-flight-vv05/.
[13] J. Doyle, A. Packard, and K. Zhou, "Review of LFTs, LMIs, and mu," in *Proceedings of the 30th IEEE Conference on Decision and Control*. IEEE, 1991.
[14] A. Marcos, S. Bennani, C. Roux, and M. Valli, "LPV modeling and LFT uncertainty identification for robust analysis: application to the VEGA launcher during atmospheric phase," *IFAC-PapersOnLine*, vol. 48, no. 26, pp. 115 – 120, 2015, 1st IFAC Workshop on Linear Parameter Varying Systems LPVS 2015.
[15] P. Simplício, S. Bennani, A. Marcos, C. Roux, and X. Lefort, "Structured singular-value analysis of the VEGA launcher in atmospheric flight," *Journal of Guidance, Control, and Dynamics*, vol. 39, no. 6, pp. 1342 – 1355, 2016.
[16] C. Roux and I. Cruciani, "Scheduling schems and control law robustness in atmospheric flight of VEGA," in *Proceedings of the International ESA Conference on Guidance, Navigation and Control Systems*, 2008.
[17] A. Hjartarson, P. Seiler, and A. Packard, "LPVTools: A toolbox for modeling, analysis, and synthesis of parameter varying control systems," *IFAC-PapersOnLine*, vol. 48, no. 26, pp. 139 – 145, 2015.
[18] D. Navarro-Tapia, A. Marcos, S. Bennani, and C. Roux, "Linear parameter varying control synthesis for the atmospheric phase VEGA launcher," in *Proceedings of the 2nd IFAC Workshop on Linear Parameter Varying Systems (LPVS)*, sep 2018.
[19] G. Balas, R. Chiang, A. Packard, and M. Safonov, *Robust Control toolbox*, 2005.
[20] S. Skogestad and I. Postlethwaite, *Multivariable feedback control: analysis and design.* John Wiley & Sons, 2005.